Optics Communications 338 (2015) 11–21

Contents lists available at ScienceDirect

Optics Communications

journal homepage: www.elsevier.com/locate/optcom

Discussion

Atmospheric compensation in free space optical communication with simulated annealing algorithm

Zhaokun Li [a], Jingtai Cao [a,b], Xiaohui Zhao [a,*], Wei Liu [a]

[a] College of Communication Engineering, Jilin University, Changchun 130012, PR China
[b] Changchun Institute of Optics, Fine Mechanics and Physics, Chinese Academy of Sciences, Changchun 130033, PR China

ARTICLE INFO

Article history:
Received 5 August 2014
Received in revised form
8 October 2014
Accepted 13 October 2014
Available online 22 October 2014

Keywords:
Free space optical communication
Atmospheric turbulence
Simulated annealing algorithm
Global optimization
Coupling efficiency

ABSTRACT

As we know that the conventional adaptive optics (AO) systems can compensate atmospheric turbulence in free space optical (FSO) communication system. Since in strong scintillation conditions, wave-front measurements based on phase-conjugation principle are undesired. A novel global optimization simulated annealing (SA) algorithm is proposed in this paper to compensate wave-front aberration. With global optimization characteristics, SA algorithm is better than stochastic parallel gradient descent (SPGD) and other algorithms that already exist. Related simulations are conducted and the results show that the SA algorithm can significantly improve performance in FSO communication system and is better than SPGD algorithm with the increase of coupling efficiency.

1. Introduction

Free space optical (FSO) communication system is widely concerned among telecommunication community for both space and ground wireless communication link. It has been mainly considered for last-mile applications [1] due to its large bandwidth potentiality, unregulated spectrum, relative low power requirement, low BER through coding techniques and easy redeployment. However, atmospheric turbulence in this system often brings phase disturbances along propagation paths that are manifested as intensity fluctuation (scintillation), beam wandering and beam broadening at receiver, which leads to significantly decrease of coupling efficiency at receiving terminal [2] and affects stability and reliability of the FSO communication system [3].

Adaptive optics (AO) system is one of the effective methods to improve beam quality by correction of wave-front distortions and has made great achievements in many applications [4–9]. In the conventional AO systems, a deformable mirror (DM) is used to compensate Hphase distortion. Generally, Shack artmann wave-front sensor (S-H sensor) [10] is used to measure optical phase deviations of incoming wave-front. Based on the wave-front aberration measured by S-H sensor, DM generates a wave-front phase to compensate the phase aberration by phase conjugation theory [11,12]. In the FSO communication system, when atmospheric turbulence is heavy or distance is long, strong scintillation will make a very different measurement for the wave-front aberration. Then the conventional AO systems, based on wave-front measurement, cannot work normally [13].

To avoid undesired wave-front measurements in strong scintillation conditions, control of the wave-front correctors (deformable mirrors) in AO system can be introduced by using recently developed control algorithm based on optimization of a system performance metric, such as SPGD algorithm. Although the concept of wave-front control without wave-front measurement has been considered in the early stages of AO technology development [14–16], it has been disregarded because of rather low control bandwidth that could be achieved even with a multi-dithering control technique [17,18]. But the situation is different today due to recent development of several novel technologies: new efficient control algorithms, their implementation with the parallel processing hard ware based on VISL microelectronics, and the emergence of high-bandwidth, wave-front correctors based on micro electro mechanical systems (MEMSs) [19]. In the study of sensorless adaptive optics used in FSO communication, one of the key problems is to find the fastest possible optimization algorithm to compensate wave-front in each frame [4,13]. In most cases, the optimization speed is limited to about 7–8 kHz by MEMS DM. The system temporal response characteristics are experimentally studied by using the method of self-induced aberrations to get coarse

* Corresponding author.
E-mail address: xhzhao@jlu.edu.cn (X. Zhao).

http://dx.doi.org/10.1016/j.optcom.2014.10.028
0030-4018/

estimation of the closed-loop bandwidth independent from atmospheric turbulence conditions [13]. With the continuous development of hardware and digital processor, the performance of the system becomes better, and the high speed compensation is realizable (about thousands of Hertz), so that the instantaneous atmospheric turbulence can be considered as static.

SA algorithm, a kind of general stochastic search algorithm, is an extension of the local search algorithm. It is different from the local search algorithm since SA algorithm can access a new smaller state in the neibourhood of current state by probability. And it is a global optimization algorithm theory. In 1953, Metropolis proposed the original SA algorithm [20] but has not made positive response until Kirkpatrick proposed a modified SA algorithm [21] in 1983 and successfully used it to solve some large-scale combinatorial optimization problem. Since modern SA algorithm can effectively solve NP complicated problem, avoid least part point and overcome dependence on initial point, it is widely used in many fields, such as VLS, production scheduling [22], control, machine learning, neural network, and image processing. In this paper, a novel SA algorithm is proposed in FSO communication system to compensate the wave-front aberration without wave-front sensors. Simulation results show that the performance of FSO communication when using our new SA algorithm is significantly improved.

This paper is organized as follows: Section 2 provides models of FSO communication system, sensorless AO system, and DM. Section 3 provides the analysis of the SA algorithm, mainly the global optimization property (compared with SPGD algorithm), and the performance of the SA algorithm in FSO communication system. In Section 4, simulations are carried out to show the improved related results of SA algorithm in FSO communication system. Finally, conclusions for this paper are given in Section 5.

2. System model

2.1. FSO communication system model

The functional block diagram of FSO communication system is shown in Fig. 1 [2].

Laser point source, taken as the transmitting terminal, emits Gaussian laser beam. Since atmospheric disturbances reduce fiber coupling efficiency at receiving terminal, communication quality is seriously affected. Sensorless AO system is used here to compensate wave-front aberrations and the related detailed description is in Section 2.2. After compensation for wave-front aberration, the laser beam is coupled into a single mode fiber. Coupling efficiency is a main indicator for FSO communication system in which higher coupling efficiency means better system performance. And another important indicator is BER. Based on theoretical analysis and simulations, the coupling efficiency of the above system can be significantly improved and its BER can also be reduced. Finally the laser signal is received by optical receiver.

2.2. Sensorless AO system model

The functional block diagram of sensorless AO communication system is shown in Fig. 2 [13].

In the sensorless AO system, laser beam passes through the beam-steering system with tracking mirror (TM) for correction of large amplitude wave-front tilts and fast-steering mirror (FSM) for correction of atmospheric-turbulence-induced tilts and jitter. Higher order wave-front aberration is compensated with MEMS DM driven by SA algorithm controller. Active mirrors of AO subsystems are depicted as transmissive elements to simplify the schematic. Fast digital camera (FDC) in image plane p' of entrance pupil is used for recording the aberrations. This AO system utilizes a 32-element piston-type DM as a wave-front corrector [19,23]. The mirror is placed on an image plane of the AO receiver system pupil plane. Generally speaking, the DMs can access KHz bandwidth and the above frequencies. Adaptive optics systems operate at high frequencies, typically several hundred to several thousand Hz.

We focus on compensation of higher order (above the 3rd order) wave-front aberration. The theoretical block diagram of wave-front aberration compensation by DM is shown in Fig. 3. In this Fig, $\varphi(r)$ is initial wave-front aberration, $u(r)$ is compensation phase $\phi(r) = \varphi(r) + u(r)$ is residual phase,J is performance metric and $\mathbf{u} = \{u_1, u_2, \cdots, u_{32}\}$ is control signal of actuators with 32-element DM. AO system mainly uses DM to correct wave-front aberration $\varphi(r)$, an imaging system to record focal spot, a performance metric analyzer to calculate system performance metric J from the data of focal spot, and SA algorithm to produce control signal $\mathbf{u}$ for DM according to the changes of J.

2.3. DM model

Based on clear aperture and separation distances between actuators in a unit circle, the normalized layout of 32-element DM actuators is shown in Fig. 4.

We approximate the influence function of DM by Gaussian Model

$$S_j(x, y) = \exp\left\{\ln \omega\left[\frac{1}{d}\sqrt{(x - x_j)^2 + (y - y_j)^2}\right]^{\alpha}\right\} \tag{1}$$

where ω is the coupling coefficient determined by the sizes of electrode actuators and the DM. (x_j, y_j) is the center coordinate of the jth actuator. d is the normalized interval between the adjacent actuators, and α is the Gaussian index. The phase compensation $u(x, y)$ generated by the deformable mirror is

$$u(x, y) = \sum_{j=1}^{32} v_j S_j(x, y) \tag{2}$$

where v_j is the jth voltage of the actuators. We can see that the numeral relationship between the phase aberration generated by the DM and voltages applied on the actuators is linear.

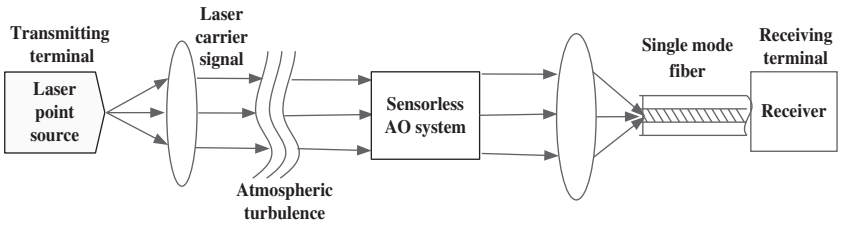

Fig. 1. Functional block diagram of FSO system.

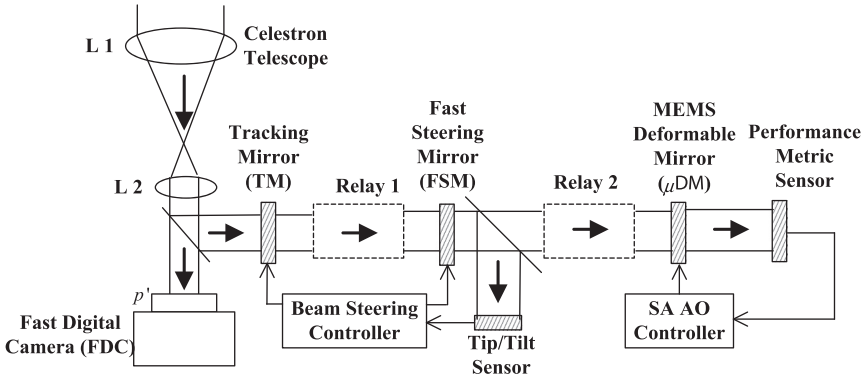

Fig. 2. Functional block diagram of sensorless AO system.

3. Analysis of SA algorithm in FSO communication system

3.1. SA algorithm

SA algorithm [25] is one of the stochastic optimization algorithms well-suited for finding a global minimum (or maximum) of some objective functions. It is based on the physical annealing process by which a solid is heated to a temperature close to its melting point, after which it is allowed to cool slowly so as to relieve internal stresses and non-uniformites [21].

For a combinatorial optimization problem, the objective is to find a solution (state) x^* to make $c(x^*) = \min c(x_i)$ for $\forall\, x_i \in \mathbf{\Omega}$, where $\mathbf{\Omega} = \{x_1, x_2, \cdots, x_n\}$ is the solution space (state space) formed by all the solutions, and $c(x_i)$ is the objective function value corresponding to the solution x_i. As a stochastic algorithm, SA algorithm works by assessing global optimal solution from any proposed solution by defining an objective function, normally a single number, whose value indicates how close that any solution is to the target. In SA algorithm, a solution x_i and the corresponding objective function value $c(x_i)$ can be regarded as a state and the corresponding energy of the object in the process of annealing temperature respectively. The optimal solution x^* is the state of the lowest energy.

In iteration of SA algorithm, Metropolis criterion [26] $p_k = \exp(\Delta J_k / T_k)$ (explained in detail in Section 3.2) is used to evaluate whether the new solution is accepted [21]. Supposing an initial temperature is equal to the heating process, finding a new solution based on Metropolis criterion is equal of the isothermal state, and gradual lowering control parameter T_k is equal to the cooling process. The corresponding relationship is given in Table. 1.

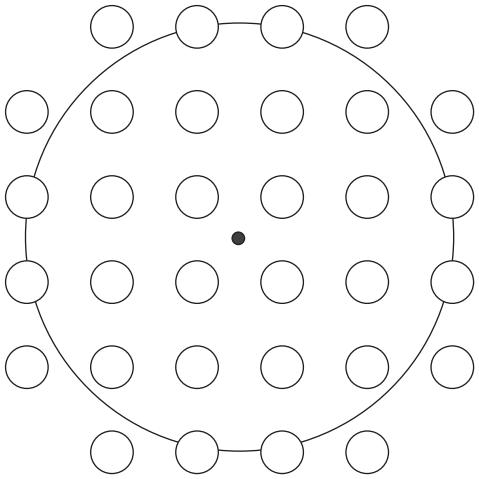

Fig. 4. Layout of 32-element deformable mirrors actuators.

Table 1
Corresponding relationship between SA and physical annealing.

SA optimization problem	Physical annealing
Solution	State
Objective function	Energy function
Optimal solution	The state of the lowest energy
Suppose an initial temperature	Heating to melting point
Find a new solution	Isothermal
Lower the control parameter $T_k$parameter	Cooling

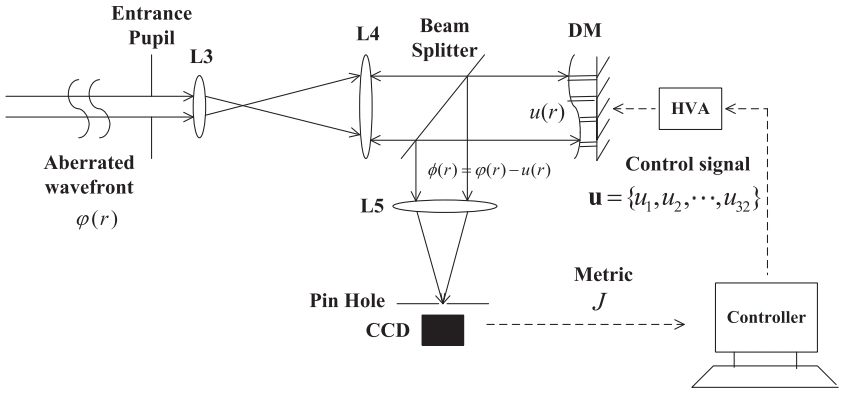

Fig. 3. Block diagram of simulation.

As an effective global optimization technique, the most important advantage of SA algorithm is that it can statistically guarantee an optimal solution. The related proofs are performed in Sections 3.3 and 3.4.

3.2. Metropolis criterion

SA algorithm consists of three functional relationships per iteration: probability density of state space of control parameters for creating perturbation vector $\Delta\mathbf{u}_k = \{\Delta u_i\}_k$; acceptance probability $p_k = \exp(-\Delta J_k/T_k)$ for deciding whether new solution is accepted or not, also called Metropolis criterion; schedule of "annealing" in annealing-time step

$$T_k = \lambda T_{k-1} \tag{3}$$

where λ the is cooling rate. The control signal, or the state mentioned before, is updated with the rule

$$\mathbf{u}_{k+1} = \mathbf{u}_k + \eta\Delta\mathbf{u}_k \tag{4}$$

where η is an adjustment coefficient called step size.

Metropolis criterion is described as follows:

Let us define an objective function

$$E_k = E(\mathbf{u}_k) \tag{5}$$

Then difference ΔJ_k can be obtained by

$$\Delta J_k = E_k - E_{k-1} = E(\mathbf{u}_k) - E(\mathbf{u}_{k-1}) \tag{6}$$

If $\Delta J_k < 0$, the new solution u_k should be accepted; If $\Delta J_k > 0$, whether the new solution is accepted or not is adjudged according to

1) If $\exp(-\Delta J_k/T_k) > \text{rand}(1)$, new solution u_k is accepted.
2) If $\exp(-\Delta J_k/T_k) < \text{rand}(1)$, new solution u_k is refused.

where rand(1) is a random number between 0 and 1.

In order to clearly describe the above problem, Metropolis criterion can also be considered as a function $M(\Delta J_k, T_k)$. If $M(\Delta J_k, T_k) \geq \text{rand}(1)$, the new state is accepted, otherwise it should be denied. After one time iteration, control parameter T_k is updated by Eq. (3). Then we obtain a new state from Eq. (4) and start next iteration. After enough numbers of iteration, we can reach global optimum.

3.3. Convergence of SA algorithm

We do not give detailed mathematical proof, but a brief explanation on the global optimality of SA algorithm [27]. According to Boltzmann function, for a specified temperature T_k, the probability of the corresponding energy E_i can be written as

$$p_i(T_k) = \frac{\exp(-(E_i/T_k))}{\sum_{j=1}^{n}\exp\left(-(E_j/T_k)\right)} \tag{7}$$

Here we suppose that n energy values $E_1, E_2, \cdots, E_n$ exist at temperature T_k, and i is a corresponding state for E_i. Taking derivative of $p_i(T_k)$ with respect to T_k, we have

$$\begin{aligned}\frac{\partial p_i(T_k)}{\partial T_k} &= \frac{\partial\left[\exp(-E_i/T_k)/\sum_{j=1}^{n}\exp\left(-(E_j/T_k)\right)\right]}{\partial T_k} \\ &= \frac{\exp(-E_i/T_k)}{T_k^2\left[\sum_{j=1}^{n}\exp\left(-(E_j/T_k)\right)\right]^2}\left[\sum_{j=1}^{n}(E_i - E_j)\exp\left(-\frac{E_j}{T_k}\right)\right]\end{aligned} \tag{8}$$

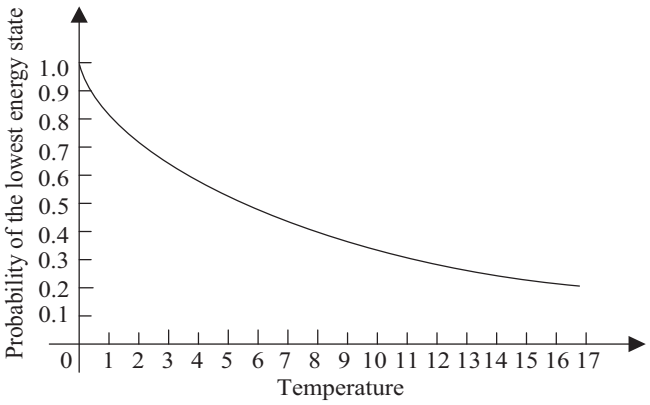

Fig. 5. Approximate curve of $p_i(T_i)$

Suppose E_{i^*} is the lowest energy value, the corresponding state is i^*. Apparently,

$$\frac{\exp(-E_{i^*}/T_k)}{T_k^2\left[\sum_{j=1}^{n}\exp\left(-(E_j/T_k)\right)\right]^2} > 0, \quad \exp\left(\frac{-E_j}{T_k}\right) > 0,$$
$$j = 1, 2, \cdots, n \tag{9}$$

thus

$$\frac{\partial p_{i^*}(T_k)}{\partial T_k} < 0, \quad \forall\, T_k \tag{10}$$

Eq. (10) shows that $p_{i^*}(T_k)$ decreases with respect to T_k. The corresponding curve is mainly of the shape given in Fig. 5.

and we can easily obtain that

$$p_{i^*}(T_k) = \frac{\exp(-(E_{i^*}/T_k))}{\sum_{j=1}^{n}\exp\left(-(E_j/T_k)\right)} = \frac{1}{\sum_{j=1}^{n}\exp\left[(-(E_j - E_{i^*})/T_k)\right]} \tag{11}$$

There exist two cases:

1) Only one global optimum state i^* exists. when $T_k \to 0$, for $\forall\, j \neq i^*$, there is

$$E_j - E_{i^*} > 0 \Rightarrow \frac{-(E_j - E_{i^*})}{T_k} \to -\infty \Rightarrow \exp\left[\frac{-(E_j - E_{i^*})}{T_k}\right] = 0$$

thus

$$\begin{aligned}p_{i^*}(T_k) &= \frac{\exp(-(E_{i^*}/T_k))}{\sum_{j=1}^{n}\exp\left(-(E_j/T_k)\right)} \\ &= \frac{1}{\sum_{j=1}^{n}\exp\left[-(E_j - E_{i^*})/T_k\right]} \\ &= 1\end{aligned} \tag{12}$$

2) N Global optimum states exist and i^* is one of them. When $T_k \to 0$, we have

$$p_{i^*}(T_k) = \frac{1}{\sum_{j=1}^{n}\exp\left[-(E_j - E_{i^*})/T_k\right]} = \frac{1}{N} \tag{13}$$

Since N global optimum states exist, the probability of the lowest energy is close to 1, when $T_k \to 0$.

Based on this discussion, when T_k is high,$-E_i/T_k$ is close to 0, $p_i(T_k) \approx 1/n$, that means when temperature is high, the probability of each state is almost equal, therefore SA algorithm starts wide

area random search. With the decrease of T_k, $p_i(T_k)$ is distributed unevenly. Finally, $T_k \to 0$, $p_{i^*}(T_k) \to 1$, which implies that SA algorithm has good ability for searching global optimum state i^*.

3.4. Global optimum of SA algorithm

To better and further understand SA algorithm, we can consider SA algorithm as a Markov chain, which is a reasonable choice because of the following reasons: SA algorithm starts from an initial state, and each state transition will select a new state j from neighborhood $N(i)$ of the present state i with the accepted state j based on Metropolis criterion $M(\Delta J_k, T_k)$ determined only by the new state j, the present state i and the parameter T_k. We should note that "select new state j" and "accept new state j" are different. We can select j by probability but do not have to accept it. If state j does not satisfy Metropolis criterion, we abandon the state j and find other new state j'.

In theoretical analysis, we neglect the limitation of the neighborhood $N(i)$ and suppose that state i can select every state wanted. The state transfer probability matrix $\mathbf{P}(T_k)$ is written as

$$\mathbf{P}(T_k) = \begin{pmatrix} p_{11}(T_k) & \cdots & p_{1n}(T_k) \\ \vdots & \ddots & \vdots \\ p_{n1}(T_k) & \cdots & p_{nn}(T_k) \end{pmatrix} \tag{14}$$

where $p_{ij}(T_k)$ is the state transfer probability form state i to state j under the condition of temperature T_k, and

$$p_{ij}(T_k) = g_{ij}(T_k)\ me_{ij}(T_k) \tag{15}$$

where $g_{ij}(T_k)$ is the selection probability of state j under the condition of state i, $me_{ij}(T_k)$ is the criterion operator based on Metropolis criterion to determine whether the new state j should be accepted or not. From the analysis above, a new selected state j is always accepted and SA algorithm starts from a wide area random search, when $T_k \to \infty$, $\mathbf{P}(T_k)$ can be written as

$$\mathbf{P}(T_k) = \begin{pmatrix} 0 & & \frac{1}{n-1} \\ & \ddots & \\ \frac{1}{n-1} & & 0 \end{pmatrix} \tag{16}$$

Considering $T_k \to 0$, we can find energy values E_i, $i = 1, 2, \cdots, n$ in ascending order

$$E_{s1} \le E_{s2} \le \cdots \le E_{sn} \tag{17}$$

And the corresponding states are si, $i = 1, 2, \cdots, n$. Apparently, $s1$ is just the global optimization state i^*. We can rewrite the state transfer probability matrix $\mathbf{P}(T_k)$ as $\mathbf{P}^*(T_k)$

$$\mathbf{P}^*(T_k) = \begin{pmatrix} p_{s1s1}(T_k) & \cdots & p_{s1sn}(T_k) \\ \vdots & \ddots & \vdots \\ p_{sns1}(T_k) & \cdots & p_{snsn}(T_k) \end{pmatrix} \tag{18}$$

where

$$p_{sisj}(T_k) = g_{sisj}(T_k)\ me_{sisj}(T_k) \tag{19}$$

When $T_k \to 0$,

$$\lim_{T_k \to 0} me_{sisj}(T_k) = \begin{cases} 0, & E_{sj} > E_{si} \\ 1, & E_{sj} < E_{si} \end{cases} \tag{20}$$

And $me_{sisj}(T_k) = 1$ means that the new state j is accepted, otherwise it is abandoned by Metropolis criterion, hence

$$p_{sisj}(T_k) = \begin{cases} 0, & E_{sj} > E_{si} \\ g_{sisj}(T_k), & E_{sj} < E_{si} \end{cases} \tag{21}$$

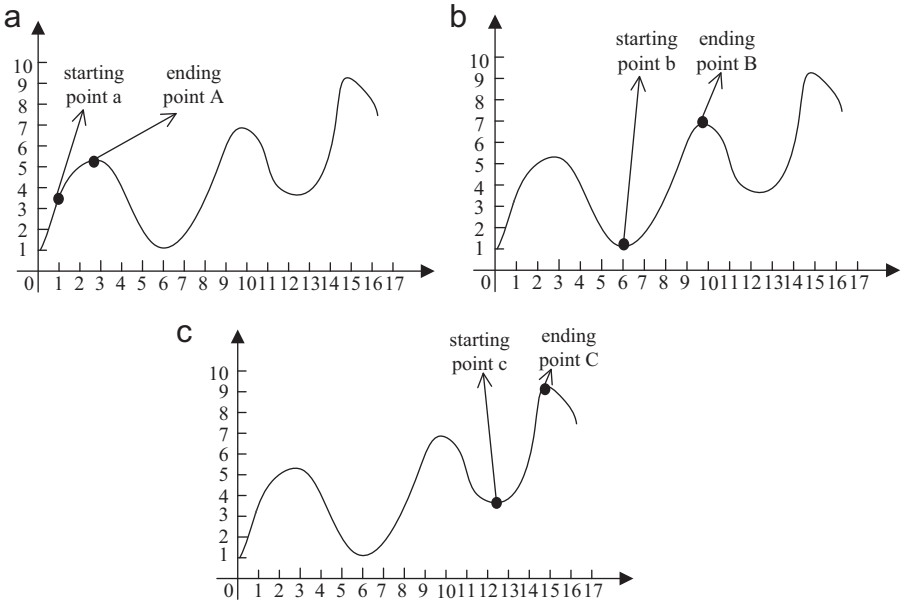

Fig. 6. Optimization by SPGD algorithm. (a) Local optimum access from starting point a. (b) Local optimum access from starting point b. (c) global optimum access from starting point c.

and

$$\mathbf{P}^*(T_k)=\begin{pmatrix} 1 & & & & 0\\ g_{s2s1}(T_k) & g_{s2s2}(T_k) & & & \\ g_{s3s1}(T_k) & g_{s3s2}(T_k) & g_{s3s3}(T_k) & & \\ \vdots & \vdots & \vdots & \ddots & \\ g_{sns1}(T_k) & g_{sns2}(T_k) & g_{sns3}(T_k) & \cdots & g_{snsn}(T_k)\end{pmatrix} \tag{22}$$

It is a down triangular matrix. It is worth to mention that the 1st row vector (1 0 0 ⋯ 0) cannot go to other states from state $s1$, when $T_k \to 0$.

When $T_k \to 0$, we define $\mathbf{\Pi}=(\pi_{s1}, \pi_{s2}, \cdots, \pi_{sn})$ is the probability vector of steady state. Then we can obtain

$$\mathbf{\Pi}=\mathbf{\Pi}\mathbf{P}^*(T_k) \tag{23}$$

Eq. (23) can be written as

$$(\pi_{s1}, \pi_{s2}, \cdots, \pi_{sn})=(\pi_{s1}, \pi_{s2}, \cdots, \pi_{sn})\cdot\begin{pmatrix} 1 & & & & 0\\ g_{s2s1}(T_k) & g_{s2s2}(T_k) & & & \\ g_{s3s1}(T_k) & g_{s3s2}(T_k) & g_{s3s3}(T_k) & & \\ \vdots & \vdots & \vdots & \ddots & \\ g_{sns1}(T_k) & g_{sns2}(T_k) & g_{sns3}(T_k) & \cdots & g_{snsn}(T_k)\end{pmatrix} \tag{24}$$

Hence we have

$$\pi_{s1}=\pi_{s1}+\pi_{s2}g_{s2s1}(T_k)+\cdots+\pi_{sn}g_{sns1}(T_k) \tag{25}$$

Thus

$$\sum_{i=2}^{n}\pi_{si}\cdot g_{sis1}(T_k)=0 \tag{26}$$

We know $\pi_{si}\geq 0$, $g_{sis1}(T_k)\geq 0$ and $g_{sis1}(T_k)>0$, therefore $\pi_{si}=0$, $i=2, 3, \cdots, n$. In other words, when $T_k \to 0$, $\mathbf{\Pi}=(1, 0, \cdots, 0)$ is the probability vector of steady state, which means when Markov process is stable, state $s1(i^*)$ is reached with probability 1.

3.5. Comparison between SA and SPGD algorithm

SPGD algorithm is used in FSO communication system to compensate wave-front aberrations [13] for comparison. SPGD algorithm has a disadvantage that may be trapped in a local optimum [28]. While SA algorithm can attain global optimum as long as the iteration number is large enough with proof in Section 3.2. Two groups of figures (Fig. 6 and Fig. 7) are given to show the difference between two optimization algorithms.

In Fig. 6, the drawback of SPGD algorithm is shown. A starting point "a" in (a) can only access local maximum ending point "A" but not global maximum "C". The reason is that when the optimization is trapped in a local maximum, the point "A" has no chance to get over the local maximum and cannot access the global maximum. This depends on the initial point, we can see that in (a) and (b), an inappropriate initial point (starting point "a" or starting point "b") leads to a bad local maximum (ending point "A" or ending point "B"), but an appropriate initial point (starting point "c") can access the global maximum "C", as shown in (c).

While Fig. 7(a–c) shows that SA algorithm can always access the global maximum no matter which initial point is chosen. Some relative simulations are performed in Section 4. Some other optimization algorithms are also proposed for sensorless adaptive optical systems. The performance of genetic algorithm (GA) is barely satisfactory since it is easily trapped in bad local optimum point its and convergence speed is low. In fact this is a common problem in the intelligent algorithms and swarm algorithms, including artificial fish swarm algorithm, shuffled frog leaping algorithm and so on. But with a high dimension search space, particle swarm optimization (PSO) is the only exception. Algorithm of pattern extraction (Alopex) is a local optimization algorithm and its convergence speed is also low. Hybrid genetic-hill climbing (HGHC) algorithm and hybrid simulated annealing-hill climbing algorithm (SAHC) are not greatly concerned currently because they do not work better than SPGD and are difficult to realize. In fact, SPGD algorithm, realized in experiment, is one of the most common ways in correcting the wavefront aberration currently.

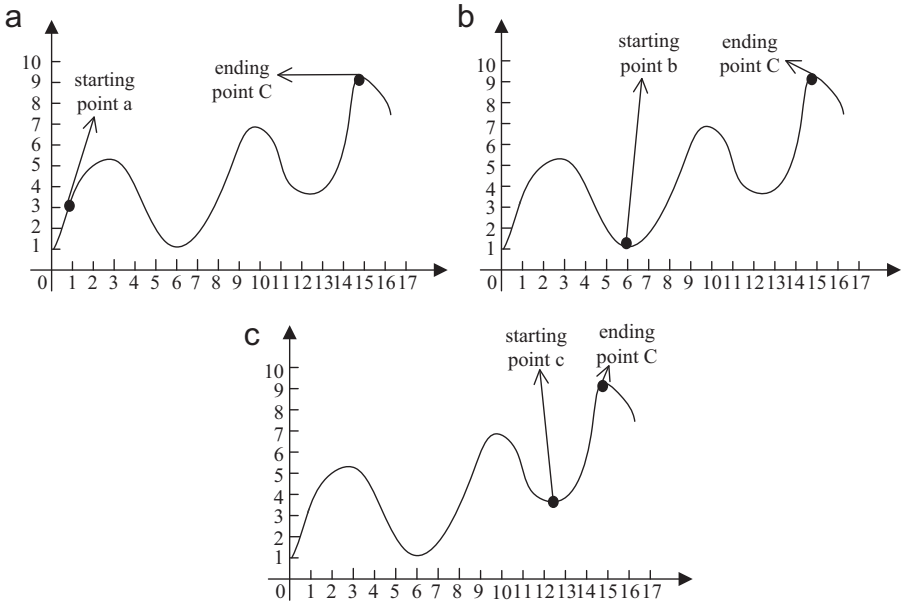

Fig. 7. Optimization by SA algorithm. (a) Global optimum access from starting point a. (b) Global optimum access from starting point b. (c) Global optimum access from starting point c.

3.6. SA algorithm in FSO communication system

In AO control of FSO communication system, SA algorithm is well suited to the task due to its ability to independently optimize many variables synchronously. Control of the DM is based on optimization of a system performance metric J by using SA algorithm. This metric is proportional to Root-Mean-Square (RMS) value of the wave-front aberration, which is conventionally used for FSO communication system.

In practice, we choose RMS value as the objective function value and try to find the global minimum. A voltage vector $\mathbf{u}$ corresponds to the "state" mentioned before.

The main flow can be described as follow:

1) Get an initial voltage vector $\mathbf{u}^* = \mathbf{u} = \mathbf{u_0} = (u_1, u_2, \cdots, u_{32})$;
2) Submit $\mathbf{u}^* = \mathbf{u}$ to DM model, then get residual wave-front RMS value R;
3) Get a new voltage vector $\mathbf{u}'$ by Eq. (4);
4) Submit $\mathbf{u}'$ to DM model, then get residual wave-front RMS value R';
5) Determine whether $\mathbf{u}'$ is accepted:
   a) $R_{k+1} < R_k$, then $\mathbf{u}'$ is accepted, $\mathbf{u}^* = \mathbf{u} = \mathbf{u}'$;
   b) $R_{k+1} \geq R_k$, then $\mathbf{u}'$ is accepted based on Metropolis criterion: if $\exp(-(R' - R)/T) > \text{rand}(1)$, $\mathbf{u}^* = \mathbf{u} = \mathbf{u}'$; if $\exp(-(R' - R)/T) < \text{rand}(1)$, $\mathbf{u}^* = \mathbf{u}$.

   If reaching the ending standard, end the iteration; otherwise, update T by Eq. (3), then go back to step 3;
6) $\mathbf{u}^*$ is the state corresponding to the global minimum.

The goal of a conventional adaptive optics system is to minimize the residual phase aberrations after the incoming wave passes the deformable mirror. This corresponds to the maximization of Strehl Ratio (ST) which is defined as the ratio of the actual maximum intensity of the zero order diffraction spot and its theoretical upper limitation for an undistorted wave.

Generally, the received laser signals are coupled into a single mode fiber, so the coupling efficiency of single mode fiber, defined as the ratio of the average power coupled into the fiber to the average power in the receiver aperture plane [29], has significant influence on the performance of FSO system. The coupling efficiency can be expressed as

$$J \propto \frac{\left|\iint A_f(r) M_0^*(r) d^2 r\right|^2}{\iint A_f(r) A_f^*(r) d^2 r \times \iint M_0(r) M_0^*(r) d^2 r} \tag{27}$$

where $A_f(r)$ is the Fourier transform of single-mode fiber optical field, $M_0(r)$ is the incident optical field in the focal plane, $A_f(r)$ and $M_0(r)$ are complex quantities. Since Eq. (12) is too complex to calculate, we apply ST to simplify the average coupling efficiency [29,30] given by

$$ST \propto \left|A_f(r_0)\right|^2 \tag{28}$$

where r_0 is the desired on-axis location of the center of the fiber. Assume that the wave-front phase aberration satisfies Gauss distribution, then ST can be estimated by variance RMS^2 as follows:

$$ST \propto \exp(-\text{RMS}^2) \tag{29}$$

When RMS^2 is close to zero, we can get an easier formula as

$$ST \propto 1 - \text{RMS}^2 \tag{30}$$

Table 2
Basic parameters of CCD.

Pixel size	$9.9\ \mu\text{m} \times 9.9\ \mu\text{m}^2$
Resolution	256×256
Frame rate	1076

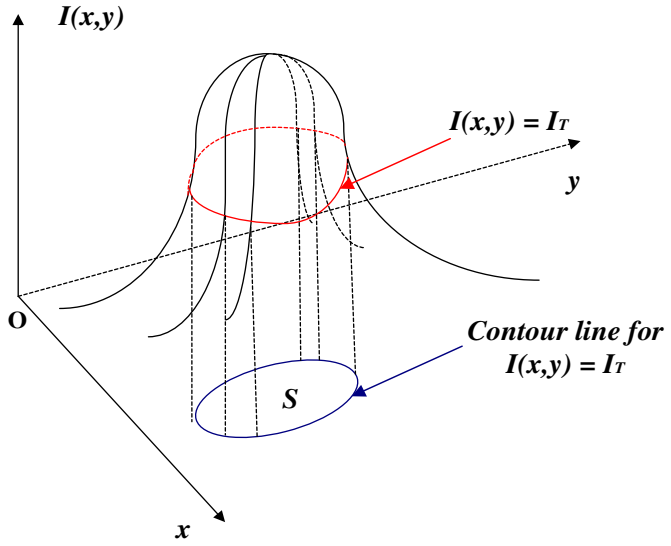

Fig. 8. Area S truncated by optical intensity of $I(x, y) = I_T$

In practice, pixel size of CCD camera approximately equals to the fiber diameter, ST is expressed as [2]

$$ST = \frac{\left|\max\left[A(i)\right]\right|^2}{\left|\sum_{i=1}^{N}\left[A(i)\right]^2\right|} \tag{31}$$

where, $A(i)$ is the gray value of the ith pixel, and N is the number of pixels. The basic parameters of CCD are shown in Table 2.

With the increase of the coupling efficiency, more energy is coupled into the single mode fiber, BER of the FSO communication system decreases significantly. In the theory analysis, without considering detector noise, BER for an on–off-keying (OOK) FSO communication system with a threshold value – an appropriate intensity I_T, can be calculated by [31]

$$\text{BER} = \frac{1}{2}P(I \leq I_T) \tag{32}$$

where $P(I \leq I_T)$ is the probability of $I(x, y) \leq I_T$, (x, y) is a pixel in the focus plane of the detector and $I(x, y)$ is the corresponding intensity. Due to regardless of the detector noise, code "0" will not be misjudged. Consequently, it cannot produce bit error. On the other hand, for code "1", when the intensity is not in area $S = \{(x, y): I(x, y) > I_T\}$, as shown in Fig. 8 [31], it will be decoded as code "0", then bit error appears. In practice, the optical intensity of the center point (0, 0) or the center area of the image, received on focus plane, is used to determine whether bit error appears. Related simulations in Section 4 show that BER in FSO communication system dramatically decreases by using SA algorithm.

4. Numeral simulations

4.1. Wave-front aberration correction with SA algorithm and comparison with SPGD algorithm

In numerical simulations, we introduce a group of original wave-front aberration and assume that the limitation of stroke is

Table 3
Zernike coefficients of introduced wave-front aberration.

Zernike order	3rd order	4th order	5th order	6th order	7th order	8th order	9th order	10th order
Zernike coefficient	1.30	0.65	−0.40	0.32	−0.45	−0.30	0.25	−0.15

enough and the receiving aperture is 120 cm, the wave-front aberration satisfies Gauss distribution without considering the noise and the energy loss of AO system, the analysis of the coupling efficiency is provided. We introduce the initial wave-front aberration with Zernike coefficients shown in Table 3. With the introduced aberration, the initial coupling efficiency is only 41.67%, that means more than half energy is lost through the propagation. The corresponding atmospheric coherent length is about 3–4 cm [32], and such small value means a strong turbulence fluctuation.

In addition, one main reason for the use of analog VLSI in the AO system is the inherent necessity of high iteration rates for the compensation of the dynamic wave-front distortions [13]. Although these self-induced-aberration experiments only give a general idea about the system behavior, we should consider them as a coarse estimation. As discussed earlier [4,13], the convergence depends on the spatiotemporal correlation of the phase distortions. This relationship cannot be modeled with self-induced aberrations. Hence the effective bandwidth for the turbulence compensation can be expected higher than the anticipated from these experiments.

Comparisons about some already existing algorithms are given in Fig. 9. We can find that these algorithms have similar results (final coupling efficiencies are about 0.88), and the convergence speeds achieve about 2000–3000 iterations. And HGHC and SAHC algorithms do not provide us interest because of local extremum and computation complexity. PSO is only at the stage of design and simulation with the problem of local extremum even it has tolerated convergence speed [33].

SPGD algorithm and SA algorithm are respectively used to compensate the wave-front aberration. In SPGD algorithm, the gain coefficient $\gamma = 0.6/(J + C)$, J is the performance metric which always is ST and $C > 0$ is a constant. Each element of the random disturbance vector $\Delta\mathbf{v}$ is independent and satisfies Bernoulli distribution, and $|\Delta v_i| = 0.09V$ $(i = 1, 2, \cdots, 32)$. While in SA algorithm, the cooling rate λ in Eq. (3) is 0.85, the adjustment coefficient η in Eq. (4) is 1.0, the perturbation vector $\Delta\mathbf{u}_k$ in each iteration is a random vector, and each element in $\Delta\mathbf{u}_k$ is 0.09 V.

Three groups of comparisons about the residual wave-front aberration between SA algorithm and SPGD algorithm are given in Fig. 10. The initial state (initial voltage vector $\mathbf{v}^{(0)}$) in each group is shown in Table 4.

All these above results show that SA algorithm performs better than SPGD algorithm in FSO AO system, due to its global optimization character. The performance of SPGD algorithm in FSO system badly depends on the initial voltage vector $\mathbf{v}^{(0)}$, it can be easily trapped in the local optimum but SA algorithm always accesses the global optimum. Note that SA algorithm may accept a "worse" state due to Metropolis criterion, which means it may perform worse than SPGD algorithm at start, but it finally does better than SPGD algorithm after enough iteration. Other conclusion from Fig. 10 is that SA has fast compensation convergence speed, which is a modest improvement compared with SPGD. After taking different platforms into account, we use iteration number to represent the convergence speed. By the selected parameters, SA has 800–900 iterations while SPGD (or some other algorithms such as PSO) needs more than 2000 iterations. Again, this is only a coarse estimation and can explain the problem to some extent. To be more concrete, SPGD has been an implemented method and the experiment results (with corresponding efficiencies) are shown in Fig. 11. We know that these experiment results are not so ideal as that given in simulation because of the device constraints.

Take initial voltage vector $\mathbf{v}^{(0)} = \{1.0, 1.0, \cdots, 1.0\}$ (as in Group1), the correcting results of SA are demonstrated in Fig. 12. Graphs (a–i) are the initial wave-front aberrations and the residual wave-front aberrations after 50, 100, 1500, 200, 500, 1000, 2000, 5000 iterations respectively.

4.2. Simulations about the performance in FSO communication system

Some corresponding normalized optical intensity character of the images received at the FSO communication system receiver is shown in Fig. 13. It is obvious that more and more energy converges in the center (0, 0) with the decrease of RMS.

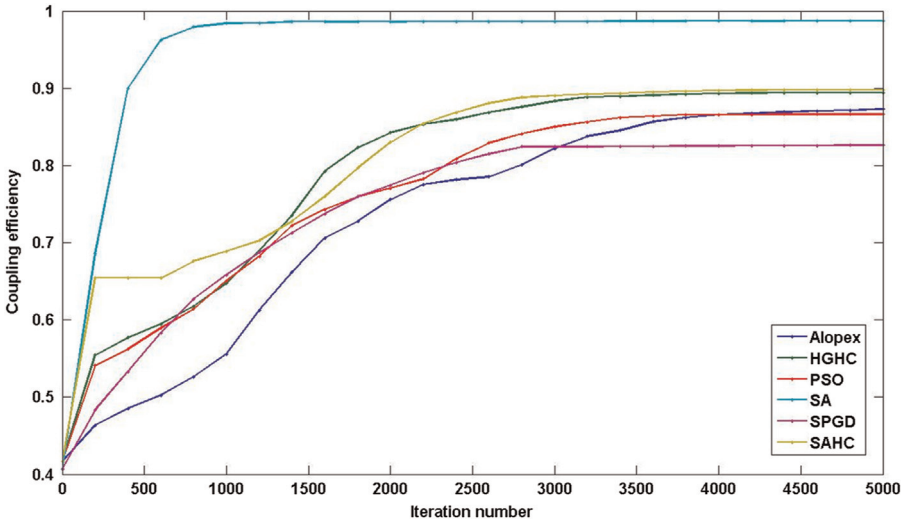

Fig. 9. Coupling efficiency with some algorithms in FSO.

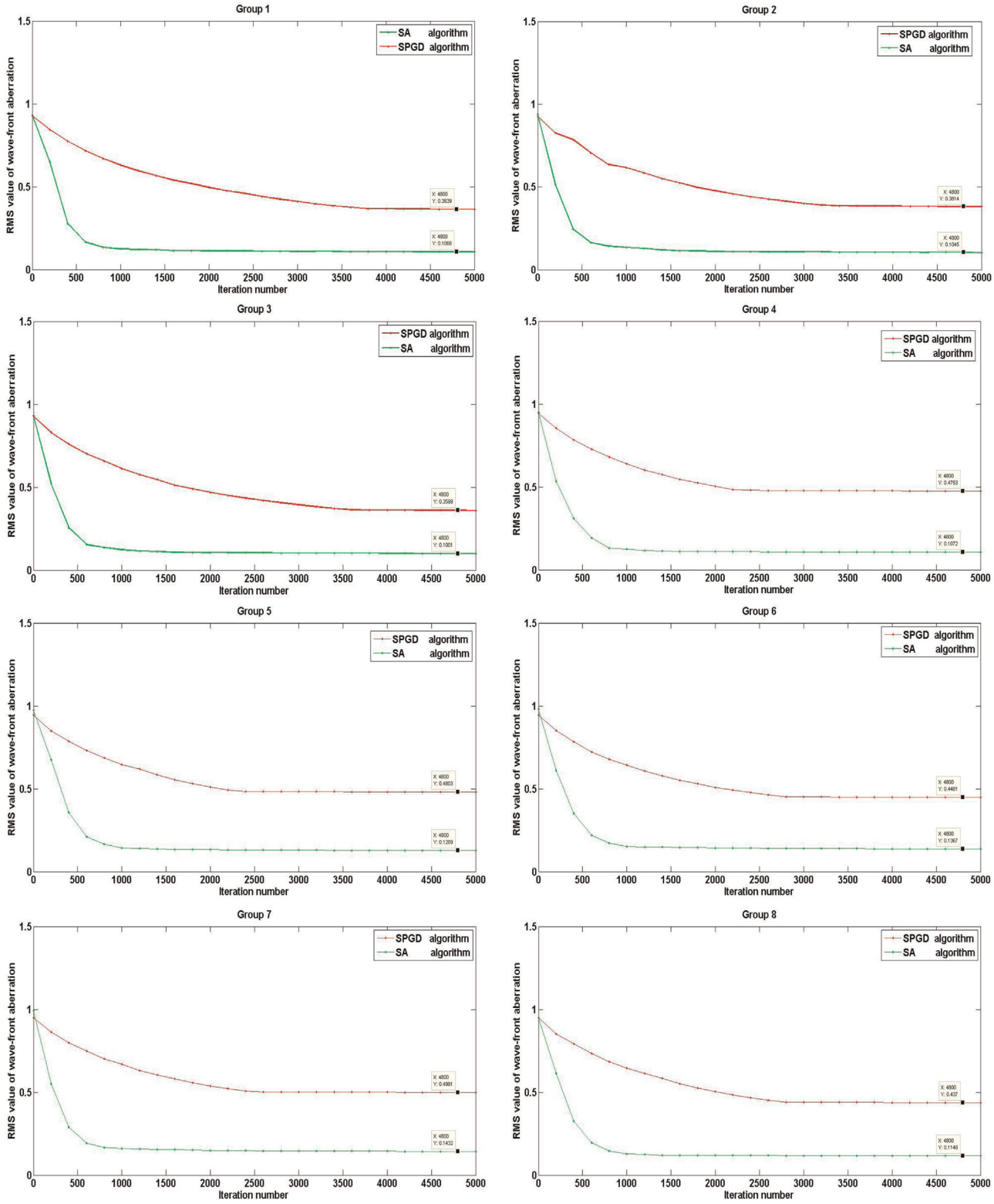

Fig. 10. Comparisons of residual wave-front aberration between SA algorithm and SPGD algorithm.

Fig. 14 shows the approximate relationship between the average coupling efficiency and the RMS of wave-front aberrations, according to Eqs. (28) and (29).

Due to the reduced RMS in residual wave-front aberrations, the coupling efficiency at the FSO receiver is improved, and the performance of the FSO communication system is significantly improved too. Detailed data of three groups based on SA algorithm and SPGD algorithm is shown in Table 5.

In addition, we have known that the single shot correction assumption is concerned for the algorithm converge speed and atmospheric time. And SPGD is a typical example in [13] with about 500 iterations in experiment, or corresponding to 50 ms. As

Table 4
Initial voltage vector in each group.

Group no.	Initial voltage vector	Group no.	Initial voltage vector
Group 1	$\mathbf{v}^{(0)}$={1.0.1.0,…,1.0}	Group 5	$\mathbf{v}^{(0)}$={1.8.1.8,…,1.8 }
Group 2	$\mathbf{v}^{(0)}$={1.5.1.5,…,1.5}	Group 6	$\mathbf{v}^{(0)}$={2.0.2.0,…,2.0}
Group 3	$\mathbf{v}^{(0)}$={0.8.0.8,…,0.8}	Group 7	$\mathbf{v}^{(0)}$={2.5.2.5,…,2.5}
Group 4	$\mathbf{v}^{(0)}$={0.5.0.5,…,0.5}	Group 8	$\mathbf{v}^{(0)}$={0.0.0.0,…,0.0}

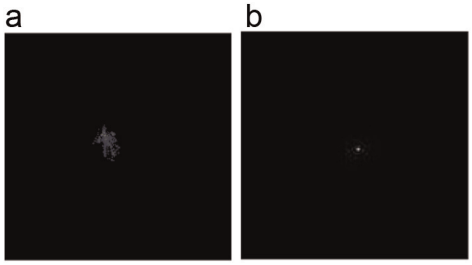

Fig. 11. Images captured by CCD. (a) Before correction (~3%) (b) After correction (65%)

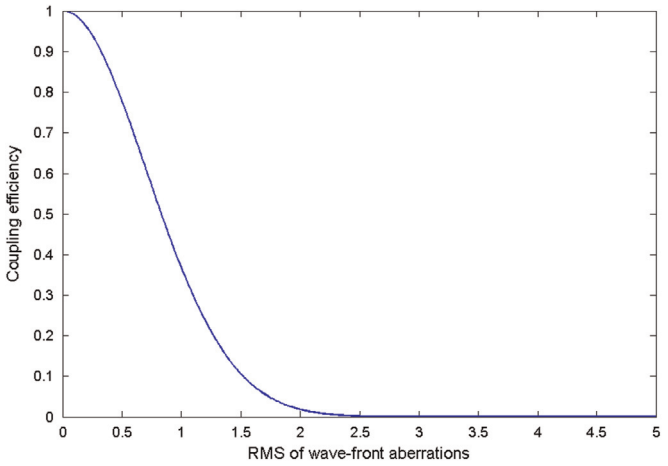

Fig. 14. Relationship between average coupling efficiency and RMS of wave-front aberrations.

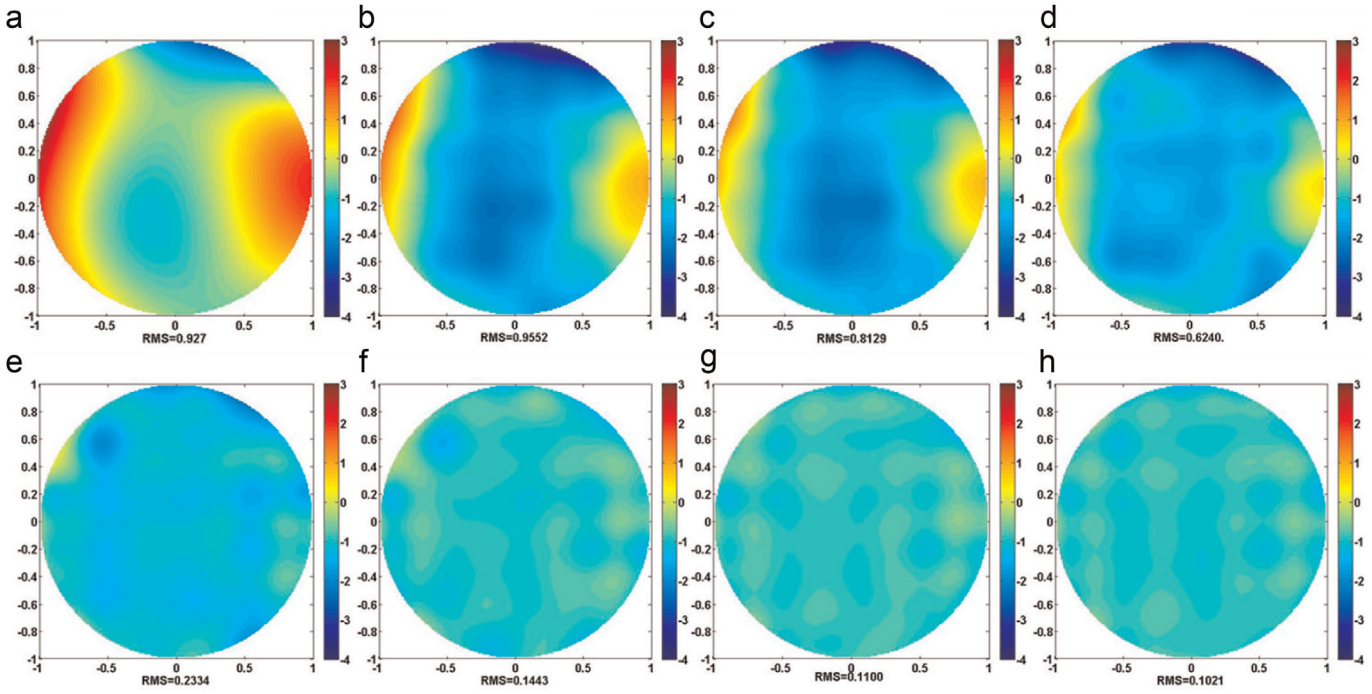

Fig. 12. Residual wave-front aberrations after different iterations.

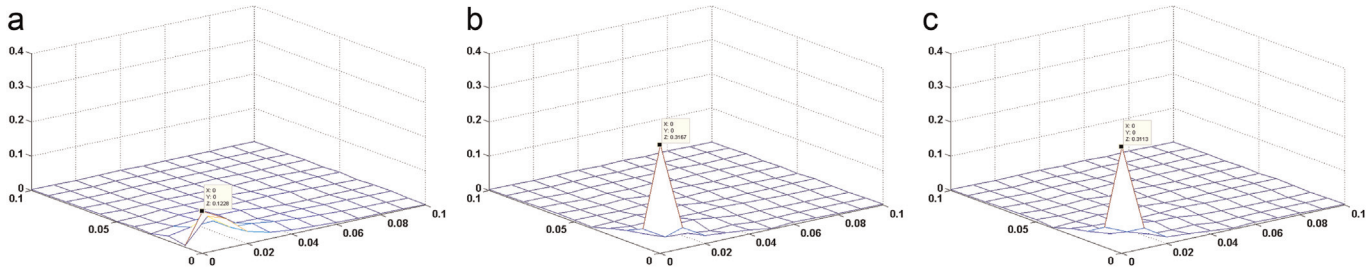

Fig. 13. Optical intensity character of the received images.

Table 5
Comparison of coupling efficiency at FSO receiver between SA and SPGD.

No.	Initial coupling efficiency (%)	Coupling efficiency with SPGD (%)	Coupling efficiency with SA (%)
1	41.67	87.60	98.87
2	–	86.46	98.91
3	–	87.85	99.00
4	–	80.00	98.86
5	–	79.42	98.35
6	–	81.82	98.15
7	–	87.60	98.87
8	–	82.64	98.69

mentioned above, the operation rate is limited by the MEMs DM (7–8 kHz), which theoretically satisfies the requirement of AO system correction. Greenwood frequency [34], an important metric to measure the character in time of the atmospheric turbulence, expresses the requirement of MEMS bandwidth. In practice we should ensure the convergence time in tens of milliseconds at the same level of atmospheric coherent time. Ideally, when the processor speed is fast enough, the atmospheric is almost static if the algorithm convergence speed is near the atmospheric coherent time. When we consider the implementation of the algorithm in practice, the parameters and the metric should be modified based on the experience of the operators and the specific circumstances. The other importance is that AO often does not directly correct the received signal but the beacon because of consideration of Nyquist principle.

5. Conclusion

In this paper, in order to guarantee the performance of FSO communication system under bad atmospheric environment, a new sensorless FSO AO system with a proposed global optimization algorithm SA is presented to compensate the wave-front aberration. Our SA algorithm can access global optimum with brief theoretical explanation and computer simulations, Therefore this FSO AO system can get better performance in the comparisons between using SA algorithm and SPGD algorithm. The compared results also show that the average coupling coefficient increases from 41.67% to more than 98%, the dissipation of energy is reduced.

Acknowledgment

This work was supported by the National Natural Science Foundation of China (No. 61171079).

References

[1] Mohammad Abtahi, Suppression of turbulence-induced scintillation in free-space optical communication systems using saturated optical amplifiers, J. Lightwave Technol. 24 (12) (2007) 4966–4973.
[2] Wei Liu, Wenxiao Shi. Free space optical communication performance analysis with focal plane based wave-front measurement, Opt. Commun. 309 (2013) 212–220.
[3] Song Dongyiel, Hurth Yoon Such, Cho Jin Woo, 4 × 10 Gb/s terrestrial optical free space transmission over 1.2 km using an EDFA preamplifier with 100 GHz channel spacing, Opt. Express 7 (2000) 280–284.
[4] Mikhail A. Vorontsov, Decoupled stochastic parallel gradient descent optimization for adaptive optics: integrated approach for wave-front sensor information fusion, J. Opt. Soc. Am. 19 (2) (2002) 356–368.
[5] Martin J. Booth, Adaptive optical microscopy: the ongoing quest for a perfect image, Light: Sci. Appl. 3 (2014) e165.
[6] Jens Schwarz, Marc Ramsey, Low order adaptive optics on Z-beamlet using a single actuator deformable mirror, Opt. Commun. 264 (1) (2006) 203–212.
[7] Chao Liu, Lifa Hu, Modal prediction of atmospheric turbulence wavefront for open-loop liquid-crystal adaptive optics system with recursive least-squares algorithm, Opt.Commun. 285 (3) (2012) 238–244.
[8] Lisa Poyneer, Jean-Pierre Véran, Predictive wavefront control for adaptive optics with arbitrary control loop delays, J. Opt. Soc. Am. A 25 (7) (2008) 1486–1496.
[9] Douglas P. Looze, Structure of LQG controllers based on a hybrid adaptive optics system models, Eur. J. Control 3 (2011) 237–248.
[10] Liu Guilin, Yang Huafeng, Experimental verification of combinational deformable mirror for phase correction, Chin. Opt. Lett. 5 (10) (2007) 559–562.
[11] Jang Mooseok, Sentenac Anne, Yang Changhuei, Optical phase conjugation (OPC)-assisted isotropic focusing, Opt. Express 21 (7) (2013) 8781–8792.
[12] Morshed Monir, J. Lowery Arthur, B. Du Liang, Improving performance of optical phase conjugation by splitting the nonlinear element, Opt. Express 21 (4) (2013) 4567–4577.
[13] Thomas Weyrauch, Mikhail A. Vorontsov, Atmospheric compensation with a speckle beacon in strong scintillation conditions: directed energy and laser communication applications, Appl. Opt. 44 (30) (2005) 6388–6401.
[14] A. Buffington, F.S. Crawford, R.A. Muller, A.J. Schwemin, R.G. Smits, Correction of atmospheric distortion with an image-sharpening telescope, J. Opt. Soc. Am. 67 (3) (1977) 298–303.
[15] S.L. McCall, T.R. Brown, A. Passner, Improved optical stellar image using a real-time phase-correction system: initial results, Astrophys. J. 211 (1977) 463–468.
[16] J.W. Hardy, Active optics: a new technology for the control of light, Proc. IEEE 66 (1978) 651–697.
[17] T.R. O'Meara, The multidither principle in adaptive optics, J. Opt. Soc. Am. 67 (1977) 306–315.
[18] J.E. Pearson, S. Hansen, Experimental studies of a deformable-mirror adaptive optical system, J. Opt. Soc. Am. 67 (1977) 325–333.
[19] T.G. Bifano, J. Perreault, P.A. Bierden, Micromachined deformable mirrors for adaptive optics, SPIE 4825 (2002) 10–13.
[20] N. Metropolis, A. Rosenbluth, M. Rosenbluth, A. Teller, E. Teller, Equation of state calculations by fast computing machines, J. Chem. Phys. 21 (1953) 1087–1092.
[21] S. Kirkpatrick, C.D. Gelatt, M.P. Vecchi, Optimization by simulated annealing, Science 220 (1983) 671–680.
[22] G.J.A. Palmer, Simulated Annealing Approach to Integrated Production Scheduling, J. Intell. Manuf 7 (3) (1996) 163–176.
[23] T.G. Bifano, J. Perreault, R. Krishnamoorthy Mali, Microelectromechanical deformable mirrors, IEEE 5 (1) (1999) 83–89.
[25] W.H. Press, S.A. Teukolsky, W.T. Vetterling, B.P. Flannery., Numerical Recipes, 2nd ed, Cambridge University Press, Cambridge, UK, 1997.
[26] N. Metropolis, A.W. Rosenbluth, M.N. Rosenbluth, A.H. Teller, E. Teller, Equation of state calculations by fast computing machines, J. Chem. Phys. 21 (1953) 1087–1092.
[27] Dingwei Wang, Intelligent Optimization Methods, Higher Education Press, Beijing, China, 2007.
[28] Yasser M. Sabry, Bassam Saadany, Diaa Khalil, Tarik Bourouina, Silicon micromirrors with three-dimensional curvature enabling lensless efficient coupling of free-space light, Light: Sci. Appl. 2 (e94) (2013) 1–9.
[29] Thomas Weyrauch, Mikhail A. Vorontsov, Fiber coupling with adaptive optics for free-space optical communication, Proc. SPIE 4489 (2002) 177–184.
[30] J. Ma, Y. Jiang, L. Tan, S. Yu, W. Du, Influence of beam wander on bit-error rate in a ground-to-satellite laser uplink communication system, Opt. Lett. 33 (22) (2008) 2611–2613.
[31] Yuqiang Yang, Qiqi Han, Liying Tan, Influence of wave-front aberrations on bit error rate in inter-satellite laser communications, Opt. Commun. 284 (12) (2011) 3065–3069.
[32] Xin Zhao, Huilin Jiang, Chen Han, Fiber coupling efficiency on focal plane spot extension caused by turbulence, Optik 124 (12) (2013) 1113–1115.
[33] Ying Chen, Yong Feng, Xinyang Li, A parallel system for adaptive optics based on parallel mutation PSO algorithm, Optik 125 (1) (2014) 329–332.
[34] D.P. Greenwood, Bandwidth specification for adaptive optics systems, J. Opt. Soc. Am. 67 (3) (1977) 390–393.